Reduced Graphene Oxide-Metal Oxide Nanohybrid for Efficient Adsorption, Photodegradation and Photoinactivation of Chemical and Microbial Contaminants

Suman Thakur, Shaswat Barua and Niranjan Karak*

Advanced Polymer and Nanomaterial Laboratory, Centre for Polymer Science and Technology, Department of Chemical Sciences, Tezpur University, Tezpur 784028, India

Abstract: Reduced graphene oxide (RGO)-semiconductor metal oxide nanohybrids at different compositions of RGO and metal oxides (ZnO and/or TiO_2) were prepared. The prepared nanohybrids were characterized by X-ray diffraction (XRD), Fourier transform infrared spectroscopy (FTIR), Raman spectroscopy and thermogravimetric analysis (TGA). These nanohybrids demonstrated a great improvement in the adsorption of heavy metal ions (As^{3+} ions) and an enhancement of photocatalytic degradation of an organic pollutant (methylene blue) over the individual nanomaterials in the presence of sunlight. The nanohybrids effectively removed As^{3+} ions within 60min from the contaminated water. The organic pollutant was efficiently degraded by the studied nanohybrids under solar light as well as direct sunlight. However, among them, RGO-TiO_2 demonstrated the best photocatalytic degradation of it under both the conditions. The best-performed nanohybrid was significantly inhibited the growth of both gram negative and positive bacteria (*Escherichia coli* and *Staphylococcus aureus*) under sunlight, though photoinactivation was more pronounced for *E. coli*. Thus, the studied nanohybrid shows a great potential as a promising water purifying material.

Keywords: Absorption, composite materials, disinfection, photocatalytic degradation.

1. INTRODUCTION

One of the most pervasive problems affecting worldwide people is insufficient access to safe and clean water and thus almost 780 million people are lacking to access safe drinking water in the world [1]. Various types of contaminants especially different heavy metals and waterborne microorganisms are entering in water supplies from different wastes [2, 3]. These contaminants pollute water and make it unsafe for public health and environment. Thus, decontamination from these chemical and microbial pollutants is highly essential to obtain safe water. Conventional water treatment technologies are unable to decontaminate the polluted water, efficiently [4-6]. Therefore, development of an effective and inexpensive method to decontaminate water from source to point-of-use is highly desirable, without further stressing the environment or imperiling human health.

In this milieu, nanotechnology may be the right approach to address the afore-stated challenge. Semiconductor nanoparticles are considered as promising materials for photodegradation of organic pollutants and photoinactivation of microorganisms from wastewater [7-9]. Among the variety of semiconductor nanoparticles, TiO_2, ZnO, and SnO_2 are considered as promising photocatalysts for their superior photocatalytic performance, easy availability, low toxicity, chemical stability, etc. [10-12] However, requirement of ultraviolet (UV) light to activate such photocatalysts greatly limits their practical applications as an additional source for such light is essential due to unavailability of adequate amount of UV light in the solar spectrum (about 2-3% is only available) [13, 14]. Therefore, researchers offer more attention to obtain an alternative visible light active photocatalyst. Numerous approaches are attempted to develop such semiconductor photocatalyst (SP) and the improvement in the efficiency is achieved by dye sensitization and doping with various metal ions as well as some special nonmetals such as nitrogen, carbon and sulfur. Thus, various carbonaceous materials such as activated carbons, carbon nanotubes and graphene based SP nanohybrids are widely used for photodegradation of contaminants with improved photocatalytic performance [15-21].

Among carbon based materials, reduced graphene oxide (RGO) has an ideal nanostructure to be paired with SP nanoparticles due to high theoretical surface area of $2600 m^2.g^{-1}$, low production cost and excellent photocatalytic activity [22]. Such high surface area of RGO enhances the photocatalytic activity of SP nanoparticles by assisting adsorption of the photodegradable contaminants and by reducing the recombination rate of photogenerated electrons and holes pairs [23]. Currently, thus the fabrication of RGO-based nanohybrid is engraved a distinct niche for photodegradation of different organic pollutants. Several well-defined SP nanohybrids such as RGO-

*Address correspondence to this author at the Advanced Polymer and Nanomaterial Laboratory, Centre for Polymer Science and Technology, Department of Chemical Sciences, Tezpur University, Tezpur 784028, India; Tel: +91 3712-273638; Fax: +91 3712-267006;
E-mail: karakniranjan@gmail.com

E-ISSN: 2311-8792/15

TiO_2 and RGO-ZnO showed remarkably enhanced photocatalytic performance in degradation of different pollutants [24-26].

In addition to that, adsorption is also the most commonly used method for decontamination of pollutants especially heavy metal ions. A great industrial benefit can be achieved due to its economic advantages, high efficiency and applicability [27]. High aspect ratio based nanomaterial such as RGO is an attractive material for this application [28]. Thus, RGO based nanohybrids with good adsorption capability of heavy metal ions are fabricated for this purpose [27-29].

Here, It is pertinent to mention that SP nanoparticles and their nanohybrids also show good photoinactivation effect against different microbes [29]. TiO_2/multiwalled carbon nanotubes (CNT) nanohybrid also showed good inactivation of bacterial endospores (*Bacillus cereus*), compared to the commercial TiO_2 nanoparticles only [30]. Another study demonstrated good visible light photoinactivation against *Escherichia coli* bacteria by the same nanohybrid [31, 32]. Thus, fabrication of a nanohybrid system is a highly desirable which can adsorb heavy metal ions, degrade organic pollutants and disinfect microorganism to provide clean and safe water. This is an alternative way to reduce the expense of water purified materials if a single material can absorb and degrade different pollutants and disinfect microorganism. There is no such report which compares all such properties for a single material.

Keeping all these in mind, RGO-TiO_2, RGO-ZnO and RGO-ZnO-TiO_2 nanohybrids were prepared with the different amount of RGO. Heavy metal ions (As^{3+}) adsorption, sunlight induced photodegradation of methylene blue and photoinactivation of microbes were evaluated for the prepared nanohybrids to check their suitability as promising water purifying materials.

2. EXPERIMENTAL

2.1. Materials

GO aqueous suspension was prepared following the modified Hummers' method as reported earlier [33]. TiO_2 nanoparticles (Sigma-Aldrich, India), zinc sulphate (Merck, India), ammonia solution (Merck, India), sodium arsenite (Merck, India), hydrochloric acid (HCl, Merck, India) and methylene blue (MB, Merck, India) were used as received without further purification. *Colocasia esculenta* leaf extract was prepared as reported earlier [33].

2.2. Preparation of TiO_2-RGO Nanohybrid

Required amount of GO and TiO_2 nanoparticles were taken in water/ethanol (50:50 v/v) system. Then, the mixture was stirred for 1h and sonicated for 10min to obtain a homogenous dispersion of GO and TiO_2 nanoparticles. After that, *C. esculenta* leaf extract (10mL) was added to the homogenous dispersion (50mL) in a single necked round bottomed flask and stirred for 8h at room temperature to reduce GO. Three different nanohybrids were prepared using different weight ratios of TiO_2 and RGO (1:1, 5:1 and 10:1) and they were coded as T_1RGO, T_5RGO, and T_{10}RGO respectively.

2.3. Preparation of ZnO-RGO Nanohybrid

In the preparation of ZnO-RGO nanohybrid, 100mL GO aqueous dispersion was taken in a single necked round bottomed flask. The required amount of $ZnSO_4$ salt was added to the GO dispersion and stirred for 30min for homogenous mixing. Then an aqueous ammonia solution (5% V/V) was added drop wise to the mixture and stirring was continued for another 3h at room temperature for the formation of $Zn(OH)_2$. Finally this mixture was calcined at 300°C for 1h to obtain ZnO-TiO_2 nanohybrid. Similar to TiO_2-RGO nanohybrid, three different nanohybrids were prepared using different weight ratio of ZnO and RGO (1:1, 5:1 and 10:1) and they were coded as Z_1RGO, Z_5RGO, and Z_{10}RGO respectively.

2.4. Preparation of TiO_2-ZnO-RGO Nanohybrid

In order to prepare this nanohybrid, required amount of $ZnSO_4$ salt and TiO_2 nanoparticles were added to 100mL GO aqueous dispersion in a single necked round bottomed flask. Then, aqueous ammonia solution (5% V/V) was dropwise added and continued stirring for another 3h at room temperature. Then the mixture was calcined at 300°C for 1h to obtain the desired nanohybrid.

2.5. Characterization

Fourier transform infrared spectra (FT-IR) were taken over the wave number range of 4000–400cm^{-1} by a Nicolet (Madison, USA) FTIR impact 410 spectrophotometer using KBr pellets. The X-ray diffraction (XRD) study was performed at room temperature (ca. 25°C) by a Rigaku X-ray diffractometer (Miniflex, UK) over a range of 2θ=10-70°. Thermogravimetric analysis (TGA) of the nanohybrids was carried out by the thermal analyzer, TGA 4000

(Perkin Elmer, USA) with a nitrogen flow rate of 30mLmin^{-1} at a heating rate of 10^{o}Cmin^{-1}. Raman spectra were taken with SPEX 1403 double monochromator coupled to a SPEX 1442. The samples were excited with an air cooled argon ion laser of wavelength 488 nm. Transmission electron microscope (TEM) analysis was performed with JEOL 2100X electron microscope at operating voltage of 200kV. Elemental analysis of the nanohybrid was also performed by energy-dispersive X-ray spectroscopy (EDS).

2.6. Heavy Metal Ions Adsorption Study

Sodium arsenite was used as a model heavy metal ion pollutant. A stock solution was prepared by dissolving 4.38mg salt into 250mL millipore water. Then the as-prepared nanohybrid was dispersed into the As^{3+} solution. After stirring for 3h, the solution was filtered and filtrate was used for metal ions analysis.

Arsenic ion removal efficiency was calculated by measuring the metal ions concentration before and after adsorption, respectively. The metal ions adsorption experiment was also carried out with different nanohybrids with the variation of time. The adsorption capacities of As^{3+} were calculated using the equation:

$$q_e = \frac{(C_D - C_e) \times V}{m} \tag{1}$$

where C_0 and C_e are the initial and equilibrium concentrations of As^{3+} (mg L^{-1}), V is the volume of the solution (L), and m is the mass of nanohybrid (mg).

To illustrate the adsorption kinetics, four kinetic models viz. pseudo-first-order, pseudo-second-order, Elovich and intra-particle diffusion model were employed. The correlation coefficient (R^2) was calculated to evaluate the suitability of different models. The R^2 value more close to one indicates a more applicable model to the kinetics of the As^{3+} adsorption. The above the four kinetic models are given in equations 2, 3, 4 and 5, respectively.

$$\log(Q_e - Q_t) = \log Q_e - \frac{k_1}{2.303} t \tag{2}$$

$$\frac{1}{(q_e - q_t)} = \frac{1}{q_e} + k_2 t \tag{3}$$

$$Q_t = \frac{1}{\beta}\ln(\alpha\beta) + \frac{1}{\beta}\ln(t) \tag{4}$$

$$Q_t = K_{dif} t^{0.5} + C \tag{5}$$

where Q_t is the solid-phase loading of metal ions in the nanohybrid at time t, Q_e is the adsorption capacity at equilibrium, k_1 is the rate constant of pseudo-first order adsorption, k_2 is the rate constant of pseudo-second-order adsorption, α and β represent the initial adsorption rate and desorption constant in Elovich model, K_{dif} indicates the intra-particle diffusion rate constant and C provides information about the thickness of the boundary layer.

2.7. Photocatalytic Organic Pollutant Degradation Test

In order to assess the sunlight induced photocatalytic ability of the nanohybrid to decontaminate organic pollutants, MB was used as a model pollutant. Firstly, 100mL aqueous MB solution (5×10^{-5}M) was mixed with 10mg of nanohybrid and stirred in dark for 30 minutes to establish the adsorption–desorption equilibrium. Then, the mixture was stirred both under the solar light and in direct sunlight. At various time intervals, 3mL of the suspension was taken out and centrifuged to separate the nanohybrid. The absorbance data was recorded for the supernatant using UV-vis spectrophotometer.

The rate of dye degradation was evaluated by plotting according to pseudo first order kinetic as follows (equation 6):

$$\ln\frac{c}{c_o} = kt \tag{6}$$

where, C_o is the initial concentration, c is the concentration of MB after time (t) and k is the first order rate constant.

2.8. Photoinactivation of Microbes

Photoinactivation effect of T_{10}RGO was assayed against *Staphylococcus aureus* (ATCC 11632) and *Escherichia coli* (ATCC 10536). Bacterial suspensions were cultured overnight at 37°C in Luria Bertani broth (HiMedia, India). The tested materials (RGO, TiO_2 nanoparticle and T_{10}RGO nanohybrid) were suspended in phosphate buffer solution by the aid of ultrasonication for 15min. Each material was added to the petri plate, containing the microbial inoculum (500µL). Then the plates were kept under sunlight (intensity~15,000 lux). Another set of experiment was carried out by incubating the microbes under complete dark condition. Microbial growth was monitored for each set of the experiment by recording the UV absorbance (at 600nm) at different time intervals. Petri plates without the tested materials were considered as controls.

3. RESULT AND DISCUSSION

3.1. Preparation and Characterization of Nanohybrid

FTIR spectroscopic analyses confirmed the reduction of GO and formation of nanohybrids. The spectra of GO, T_{10}RGO, and Z_{10}RGO nanohybrids are shown in Figure **1**(**a**). After reduction of GO, broadness of OH stretching band at 3410cm^{-1} was diminished and stretching band of C=O bond at 1710cm^{-1} was completely vanished [33]. These suggest that oxygenating groups of GO are reduced in the nanohybrid. Also, the presence of Ti–O and Zn–O stretching vibration bands at 660 and 457cm^{-1}, respectively indicate the existence of TiO_2 and ZnO nanoparticle in their nanohybrids [34].

Raman spectroscopy is one of the most valuable techniques to analyze the ordered/disordered structures of carbonaceous materials and metal oxides. Figure **1**(**b**) shows Raman spectra of GO, Z_{10}RGO, and T_{10}RGO. In the spectra of Z_{10}RGO and T_{10}RGO, the increased in intensity ratio of D and G bands (I_D/I_G) from 0.88 to 1.09 and 1.14, which reflects the reduction of GO [27]. These bands are attributed to the local defects/disorders and the sp^2 graphitic structure, respectively. The existence of the 2D peak in the Raman spectra of GO and nanohybrids at ~2690cm^{-1} indicates the presence of multilayer graphene sheets. Also, peaks at 439 and 635cm^{-1} in the Raman spectra of nanohybrid are assigned to the presence of ZnO and anatase TiO_2 [35, 36].

XRD patterns of TiO_2, ZnO nanoparticles and their nanohybrids are shown in Figure **1**(**c**). In XRD patterns of TiO_2 and its nanohybrid the peaks at 25.3, 37.9, 48.0, 54.4, 56.6, and 62.8° are assigned for (101), (004), (200), (105), (211) and (204) planes of anatase TiO_2, respectively [14]. Similarly, peaks at 31.67, 34.31, 36.14, 47.4, 56.5, 62.73, 67.91 and 69.03° of ZnO nanostructure and its nanohybrid are due to (100), (002), (101), (102), (110), (103), (112) and (201) planes, respectively [12]. There was no distinct peak found for RGO in the nanohybrid. This may be due to the presence of less crystalline RGO than TiO_2 and ZnO.

TGA thermograms as shown in Figure **1**(**d**) of TiO_2, ZnO and their nanohybrids demonstrated only a marginal weight loss over the studied temperature

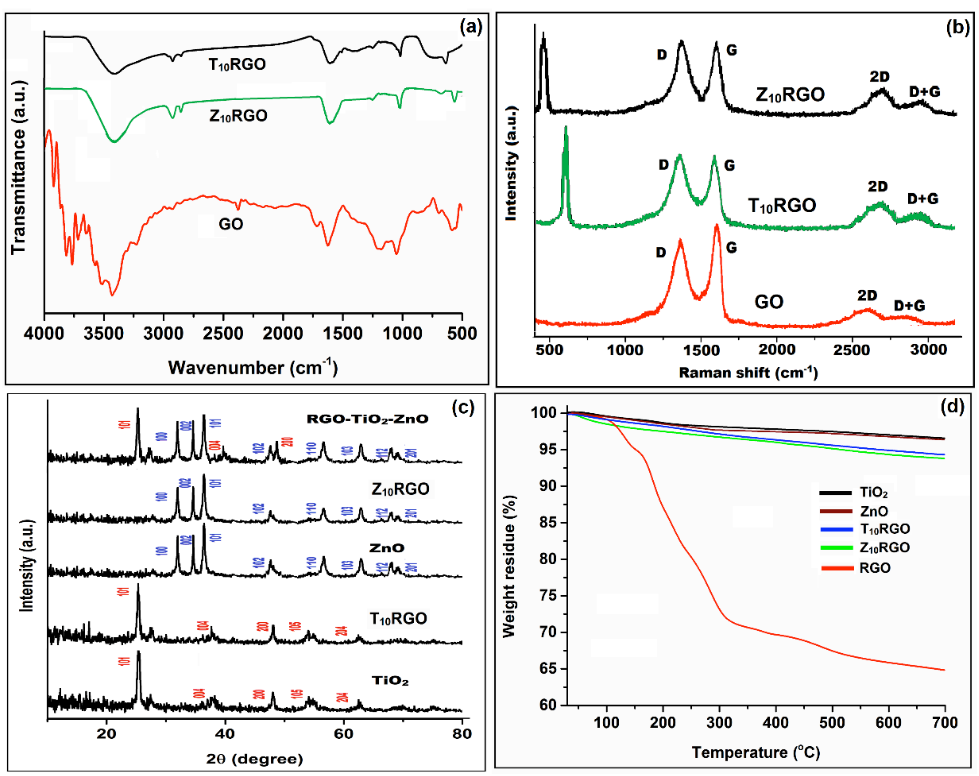

Figure 1: (**a**) FTIR and (**b**) Raman spectra of GO, T_{10}RGO and Z_{10}RGO nanohybrid; (**c**) XRD patterns of TiO_2 nanoparticles, ZnO nanoparticles, T_{10}RGO, Z_{10}RGO and TiO_2-ZnO-RGO nanohybrid, and (**d**) TGA thermograms of TiO_2 nanoparticles, ZnO nanoparticles, RGO, T_{10}RGO and Z_{10}RGO.

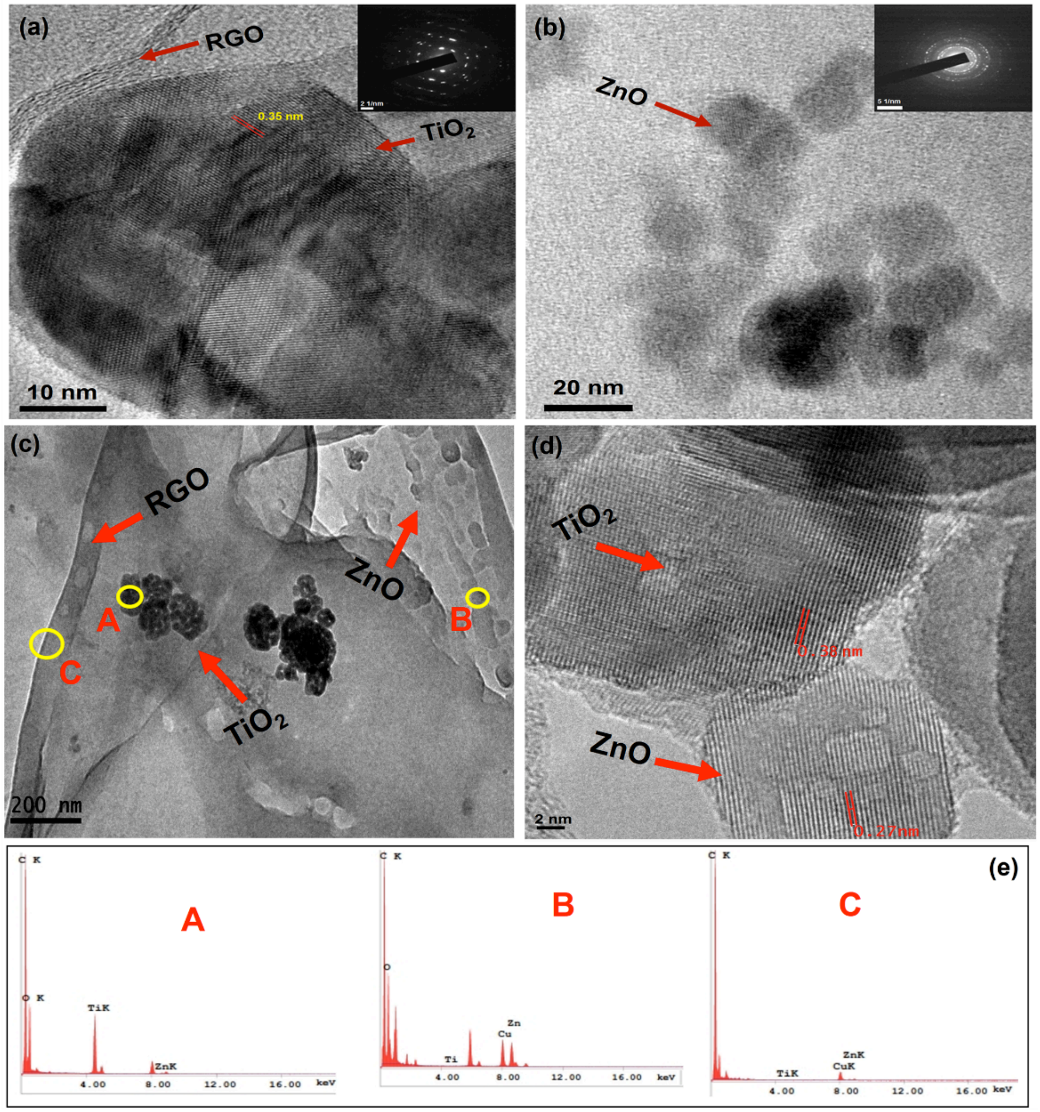

Figure 2: HRTEM images of (**a**) T_5RGO, (**b**) Z_5RGO, (**c**) and (**d**) TiO_2-ZnO-RGO nanohybrid; and (**e**) EDS of TiO_2-ZnO-RGO nanohybrid.

range. In contrary, pristine RGO demonstrated a significant weight loss in its thermogram as it contains a few amount of oxygenating group which are degraded at the higher temperature [33]. Weight loss of TiO_2 and ZnO nanoparticle are attributed to the loss of the adsorbed H_2O and the crystallization of amorphous metal oxide nanoparticles.

HRTEM images of T_5RGO and Z_5RGO nanohybrids demonstrated that TiO_2 and ZnO nanoparticles are well-dispersed on the surface of the RGO sheets (Figure **2**). The crystal lattice fringes with d-spacing of 0.35nm corresponding to the (101) plane of the anatase TiO_2 are shown in Figure **2**(**a**). This suggests that the TiO_2 nanoparticles were well-ordered structure and also the SEAD pattern indicates the presence of a high degree of crystallinity (Inset image). Similar to T_5RGO nanohybrid, Z_5RGO nanohybrid also shows a well-decorated structure with a high degree of crystallinity. The presence of the (101) plane of the anatase TiO_2 and (001) planes in the ZnO nanoparticles suggests the formation of TiO_2-ZnO-RGO nanohybrid (Figure **2c** and **2d**). Elemental compositions were also determined at different marked locations (A, B and C of Figure **2**) of TiO_2-ZnO-RGO nanohybrid as shown in Figure **2e**. EDS patterns confirmed the presence of TiO_2 and ZnO nanoparticles on the RGO sheets.

3.2. Heavy Metal Ions Adsorption Study

The kinetics of the adsorption process was investigated in order to evaluate heavy metal ions removal efficiency of the nanohybrid from the polluted water. The effect of exposure time on the adsorption of As^{3+} was performed under ambient conditions. The initial adsorption rate of metal ions was high in case of the nanohybrid as shown in Figure **3**. About 90% of As^{3+} removal was observed during the initial period of 30min in T_1RGO and Z_1RGO nanohybrids.

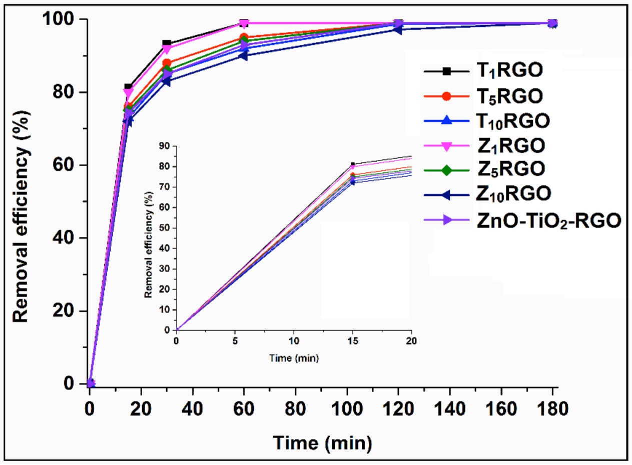

Figure 3: As^{3+} removal efficiency of the as-prepared nanohybrids with variation of time.

Then, there was a progressively decreased in removal rate and reached an equilibrium condition with almost complete metal ions removal within 60min. Other nanohybrids took little more time compared to these two nanohybrids (T_1RGO and Z_1RGO). This results clearly reflect that the amount of RGO in the nanohybrids significantly effect the adsorption of metal ions. The presence of high amount of RGO in the nanohybrid facilitates in the rapid adsorption of heavy metal ions. This may be due to high surface area and two dimensional architecture of RGO. The effective adsorption of As^{3+} on the surface of nanohybrid might be attributed to two factors: (1) a strong interaction between metal ions and the functional group present in the surface of RGO sheets and (2) an electrostatic attraction between the free exposed surface of the nanohybrid and the metal ions [27, 29].

Four kinetic models viz. pseudo-first-order, pseudo-second-order, Elovich and intra-particle diffusion model were used to study of the adsorption kinetics. The results achieved by fitting experimental data of the adsorption in these models are tabulated in Table **1**. Pseudo-second-order model fitted well with an excellent correlation coefficient for the adsorption of As^{3+} by the nanohybrids. The slopes and the intercepts of each linear plot are used to calculate the kinetic parameters for adsorption of As^{3+} (Table **1**).

The reusability of the nanohybrid for the adsorption of As^{3+} is a vital factor to acquire a cost efficient heavy metal ion absorbent. The recycling of nanohybrid was performed by washing out the bound metal ions from the surface of nanohybrid with 2M HCI solution followed by rinsing with Milli-Q water. After that, the nanohybrid was dried at 60°C and reused again. From Figure **4**, it is cleared that the adsorption capacity of As^{3+} minutely declines with increasing cycle of reuse. Even after the fourth cycle of recycling the efficiency is significantly good. This indicated that nanohybrid has a good reusability in heavy metal ion decontamination. Therefore, these materials are economically feasible for absorption of heavy metal ion.

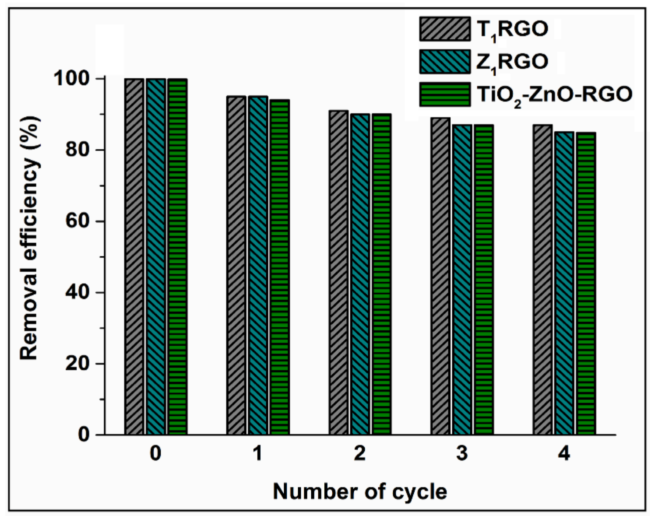

Figure 4: Metal ions removal efficiency at different cycles.

3.3. Photocatalytic Degradation of Dye

Photocatalytic degradation of organic pollutant (MB) was investigated under exposure of solar light and direct sunlight to evaluate decontamination efficiency of

Table 1: Kinetic Parameters Obtained from Different Models

Nanohybrids	Pseudo-First-Order		Pseudo-Second-Order		Elovich			Intraparticle Diffusion		
	k	R^2	k	R^2	α	B	R^2	K_{dif}	C	R^2
T_1RGO	0.65	0.933	1.21	0.987	2.19	2.63	0.941	0.06	1.86	0.912
Z_1RGO	0.52	0.941	1.03	0.982	2.10	2.4	0.932	0.05	1.72	0.923
TiO_2-ZnO-RGO	0.42	0.927	1.09	0.990	1.8	2.3	0.946	0.05	1.63	0.927

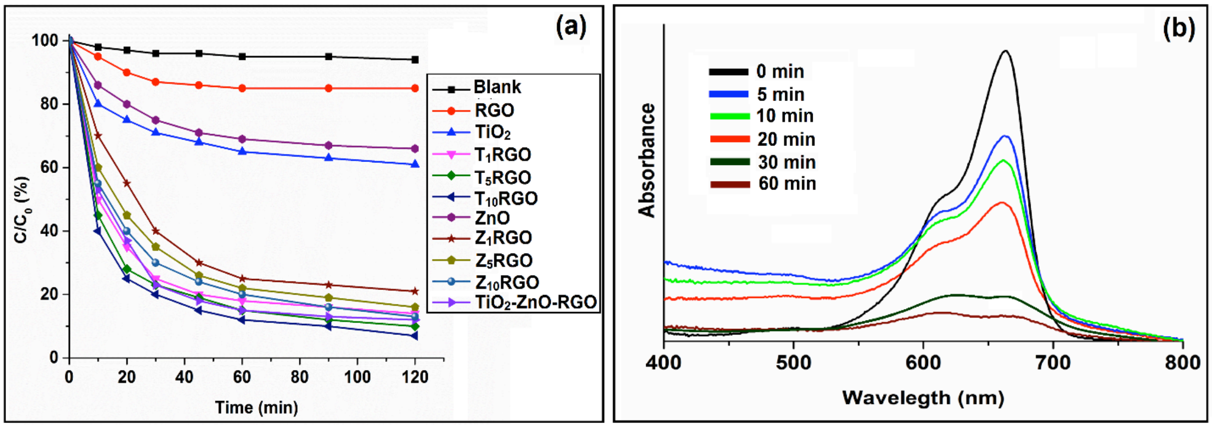

Figure 5: (**a**) Photo-decontamination efficiency of the prepared nanohybrids as a function of irradiation time where C_0 and C are the initial and actual concentration of organic pollutant at different reaction times, respectively and (**b**) Time-dependent absorption spectra of organic pollutant solutions in the presence of T_{10}RGO nanohybrid under solar light.

the prepared nanohybrid. The dye solution with the nanohybrid was kept for 30min in the dark to attain the absorption-desorption equilibrium between them before the irradiation of sunlight. Figure **5a** displays the decontamination efficiencies with different nanohybrids after 120min of solar light exposure under ambient condition. The decontamination activities of TiO_2, ZnO nanoparticles, and RGO were also measured under the same reaction conditions for comparison purpose. The concentration of MB was very minutely changed (around 8% during 2h exposure) without the use of any photocatalyst. A similar phenomenon was also demonstrated by MB in the presence of RGO.

The decontamination efficiency was remarkably enhanced in case of nanohybrids compared to individual photocatalyst nanoparticles (TiO_2 and ZnO). In comparison, TiO_2-RGO nanohybrid performed better than ZnO-RGO and ZnO-TiO_2-RGO nanohybrids. The rate constants for the MB dye degradation are 8.9×10^{-3}, 4.7×10^{-3} and 5.4×10^{-3}min^{-1} for TiO_2-RGO, ZnO-RGO and ZnO-TiO_2-RGO nanohybrids, respectively. The nanohybrid exhibited composition dependent decontamination efficiency and T_{10}RGO nanohybrid showed the best efficiency.

Figure **5b** shows the photocatalytic decontamination efficiency of T_{10}RGO nanohybrid as a function time under the solar light. T_{10}RGO nanohybrid completely degraded MB within 10min under irradiation of direct sunlight and 120min under the solar light. It is well-known that RGO possesses a giant π-conjugational plane which provides enough available surface for the interaction of organic pollutant (MB dye) through a π-π stacking with a face-to-face orientation [14]. Therefore, RGO acts as an electron acceptor and allows to quickly transfer the photoexcited electrons from the conduction band of SP to RGO in the nanohybrid. Thus, the rate of recombination of the photogenerated electron-hole pairs is suppressed and leaves more charge carriers

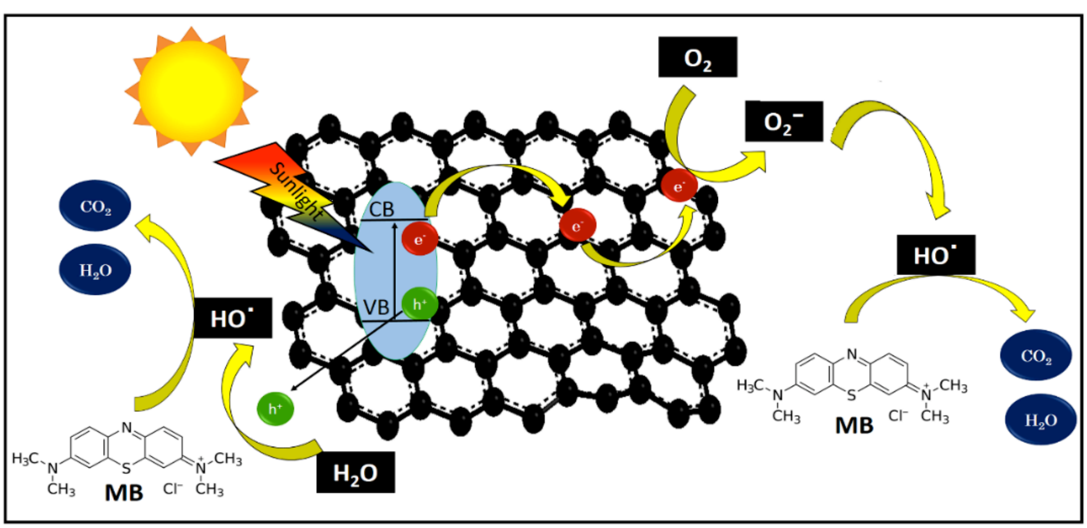

Figure 6: Proposed mechanism of organic pollutant degradation.

which form more reactive oxygen species (ROS). This eventually enhances photocatalytic decontamination activity of the nanohybrid and promotes the degradation of organic pollutants [14].

The proposed mechanism of organic pollutant degradation is shown in Figure **6**. The mechanism involves three steps and these are the adsorption of the pollutant, absorption of light by the photocatalyst and charge transfer reactions to create radical species for the decomposition of the organic pollutant [12]. Upon irradiation of SP with sunlight, valence electrons of SP are excited to the conduction band and generated holes in the VB. Different degradation efficiencies of nanohybrids can be explained by considering the work function of MB (-5.67 eV), excited MB (-3.81 eV), RGO (-4.42 eV), TiO_2 (-4.4 eV) and ZnO (-4.3 eV).

During sunlight irradiation on TiO_2-RGO nanohybrid, electron-hole pairs generated in TiO_2 nanoparticles and are present on the surface of RGO. These photoexcited electrons then transferred to RGO surface easily as the difference in work function between RGO and TiO_2 is marginal. The trapped electrons on RGO sheet react with the dissolved oxygen to form ROS as shown in Figure **6**. Also, photoexcited electrons presence on TiO_2 surface can also be trapped directly by the dissolved oxygen to form ROS. The generated ROS react with water to form hydroxyl radicals. Then, organic pollutant (MB dye) is degraded by these hydroxyl radicals through chain reactions to decompose into small molecules (as shown in Figure **6**). On the other side, holes generated in the VB of TiO_2 react with absorbed water to form surface hydroxyl radicals which then degrade the pollutant to nontoxic compounds. Also, the generated holes can directly oxidize the dye molecules. In ZnO-RGO and ZnO-TiO_2-RGO nanohybrids, the difference of work function between ZnO and RGO is large. As a result transfer of the electron to RGO sheet decreases and is directly reflected in degradation efficiencies of these nanohybrids.

Similarly to adsorption test, recyclability of the nanohybrid was checked as a photocatalyst for degradation of organic contaminant. Even 3rd cycles, the efficiency remained almost constant (Figure **7**). This indicates the tremendous potential of the nanohybrid as a reusable photocatalyst for degradation of organic pollutants.

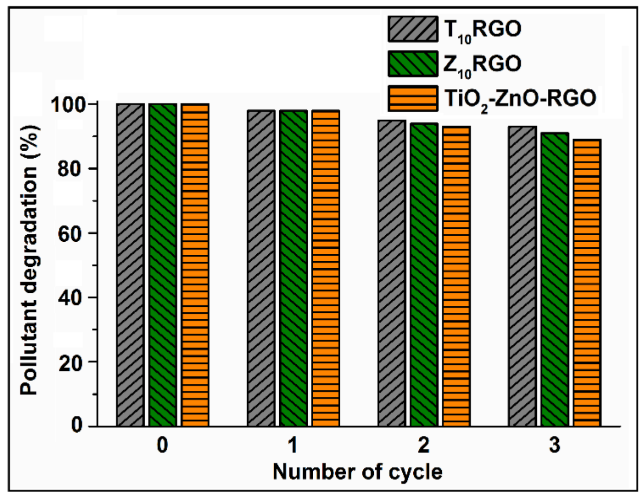

Figure 7: Organic pollutant decontamination efficiency at different cycles.

3.4. Photoinactivation of Bacteria

Photoinactivation of bacteria was investigated by using T_{10}RGO nanohybrid against *S. aureus* and *E. coli* under sunlight as well as dark. Here, only T_{10}RGO nanohybrid was tested as it showed the best

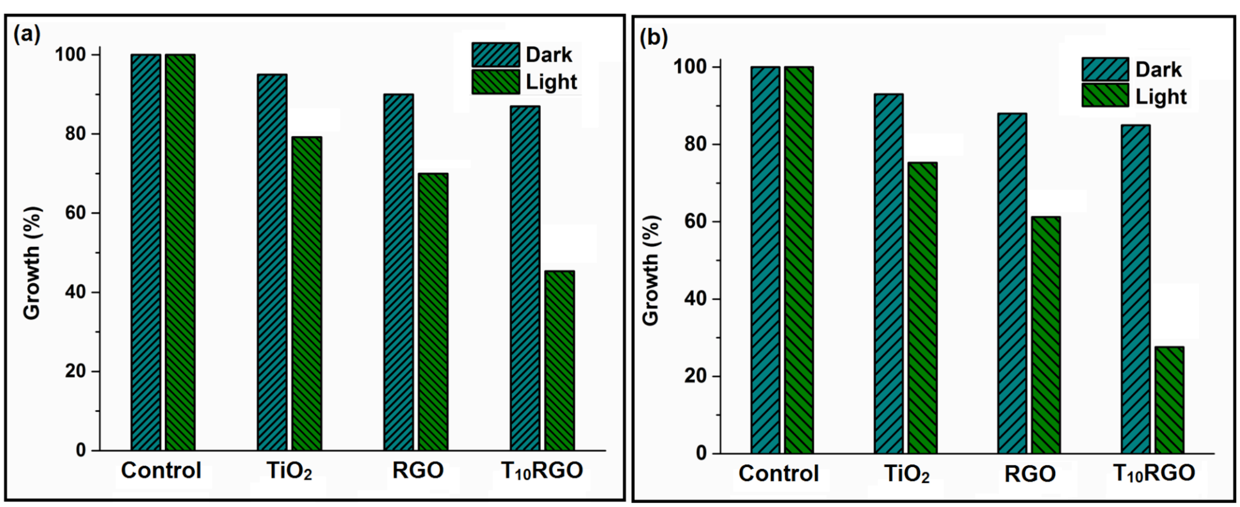

Figure 8: Growth rate of (**a**) *S. aureus* and (**b**) *E. coli* under sunlight and dark.

photocatalytic effect under the exposure of sunlight. Photoinactivation activity of RGO and pure TiO_2 nanoparticles also carried out to have a benchmark result. The percentages of growth of the bacteria in the respective culture media under both conditions (sunlight and dark) were studied as shown in Figure **8**. The significant decrease in the percentage of growth of the bacteria was noticed for T_{10} RGO nanohybrid under the exposure of sunlight for 4h. RGO and TiO_2 nanoparticles also showed similar results, however, the effect on bacteria was comparatively less than the nanohybrid. This observation clearly demonstrated that the incorporation of TiO_2 nanoparticles in RGO sheet significantly enhanced the photoinactivation activity against the tested microbes. The effect of the nanohybrid was more pronounced for *E. coli* than *S. aureus*. The presence of differential cellular receptors on the membranes of the microorganisms is attributed to such effect. It is established that RGO and TiO_2 nanoparticles both showed efficient photocatalytic and antimicrobial activities [30, 37]. From the result, it is also cleared that photoinactivation activity of nanohybrid is improved in the presence of sunlight compared to the dark condition.

During exposure of sunlight on nanohybrid, electron-hole pairs generated as shown in Figure **6**. These generated holes split the water molecules which are present in the culture medium into H^+ and OH^- ions. Dissolved oxygen molecules in the culture medium also react with the generated electron and formed superoxide radical anions ($^{\bullet}O_2^-$). These superoxide radical anions again react with H^+ ions to produce $^{\bullet}O_2H$ radicals. These radical upon subsequent collision with electrons and H^+ ions formed H_2O_2 molecules. The generated ROS especially $^{\bullet}OH$ and $^{\bullet}O_2^-$ ions cannot penetrate the microbial cell membrane as they are charged particles [38]. Therefore, they only remain in direct contact with the outer surface of the microbes; however, H_2O_2 molecules can penetrate the cell membrane and kill them [38]. Thus, the presence of nanohybrid in the culture medium effectively hinders the growth of the microbes. Nanomaterials possess the uneven surface due to rough edges and corners which provide abrasive surface texture. This rough surface contributes to the mechanical damage of the cell membrane of microbes [39]. So, even RGO can kill the microbes without the photocatalyst to a certain extent.

4. CONCLUSION

In summary, RGO-semiconductor metal oxide nanohybrids were successfully fabricated. The prepared nanohybrids were used as pollutant absorbents and sunlight induced photocatalysts for degradation of the organic pollutant as well as photoinactivation of microbes to obtain safe and clean water. Both the prepared RGO-TiO_2 and RGO-ZnO nanohybrids effectively removed the heavy metal ions (As^{3+}) within 60min with good recyclability and rapidly degraded the organic pollutant in the presence of sunlight. RGO-TiO_2 nanohybrid also pronounced photoinactivation effect against different microbes. Therefore, RGO-TiO_2 nanohybrid shows tremendous potential to decontaminate the chemical and microbial pollutants present in wastewater and might be used as a promising water purifying material. As, a single material can effectively decontaminate the chemical and microbial pollutants, the cost of purified materials also reduces.

ACKNOWLEDGMENT

S. T. Sincerely acknowledges the receipt of his Senior Research Fellowship from the Council of Scientific and Industrial Research (CSIR), India. The authors express their gratitude to SAP (UGC), India through grant No. F.3-30/2009(SAP-II).

REFERENCES

[1] Bongaarts J, Maulden WP and Phillips JF. The demographic impact of family planning programs. Stud Fam Plann 1990; 21(6): 299-10. http://dx.doi.org/10.2307/1966918

[2] Shannon MA, Bohn PW, Elimelech M, Georgiadis JG, Mariñas BJ and Mayes AM. Science and technology for water purification in the coming decades. Nature 2008; 452: 301-10. http://dx.doi.org/10.1038/nature06599

[3] Liga MV, Bryant EL, Colvin VL and Li Q. Virus inactivation by silver doped titanium dioxide nanoparticles for drinking water treatment. Water Res 2011; 45: 535-44. http://dx.doi.org/10.1016/j.watres.2010.09.012

[4] Montgomery MA and Elimelech M. Water and sanitation in developing countries: including health in the equation– millions suffer from preventable illnesses and die every year. Environ Sci Technol 2007; 41: 17-24. http://dx.doi.org/10.1021/es072435t

[5] Wintgens T, Salehi F, Hochstrat R and Melin T. Emerging contaminants and treatment options in water recycling for indirect potable use. Water Sci Technol 2008; 57: 99-107. http://dx.doi.org/10.2166/wst.2008.799

[6] Lu J, Zhang T, Ma J and Chen Z. Evaluation of disinfection by-products formation during chlorination and chloramination of dissolved natural organic matter fractions isolated from a filtered river water. J Hazard Mater 2009; 162: 140-5. http://dx.doi.org/10.1016/j.jhazmat.2008.05.058

[7] Yanga H and Cheng H. Controlling nitrite level in drinking water by chlorination and chloramination. Sep Purif Technol 2007; 56: 392-6. http://dx.doi.org/10.1016/j.seppur.2007.05.036

[8] Li Q, Mahendra S, Lyon DY, Brunet L, Liga MV, Li D, *et al.* Antimicrobial nanomaterials for water disinfection and

microbial control: potential applications and implications. Water Res 2008; 42: 4591-602.
http://dx.doi.org/10.1016/j.watres.2008.08.015

[9] Gupta VK, Jain R, Agarwal S, Nayak A and Shrivastava M. Photodegradation of hazardous dye quinoline yellow catalyzed by TiO_2. J Colloid Interface Sci 2012; 366: 135-40.
http://dx.doi.org/10.1016/j.jcis.2011.08.059

[10] Han F, Kambala VSR, Srinivasan M, Rajarathnam D and Naidu R. Tailored titanium dioxide photocatalysts for the degradation of organic dyes in wastewater treatment: a review. Appl Catal A 2009; 359: 25-40.
http://dx.doi.org/10.1016/j.apcata.2009.02.043

[11] Zhang J, Xu Q, Feng Z, Li M and Li C. Importance of the relationship between surface phases and photocatalytic activity of TiO_2. Angew Chem Int Ed 2008; 47: 1766-9.
http://dx.doi.org/10.1002/anie.200704788

[12] Wu D, Wang W, Tan F, Sun F, Lu H and Qiao X. Fabrication of pit-structured ZnO nanorods and their enhanced photocatalytic performance. RSC Adv 2008; 3: 20054-9.
http://dx.doi.org/10.1039/c3ra42874e

[13] Zhou H, Zhang H, Wang Y, Miao Y, Gu L and Jiao Z. Self-assembly and template-free synthesis of ZnO hierarchical nanostructures and their photocatalytic properties. J Colloid Interface Sci 2015; 448: 367-73.
http://dx.doi.org/10.1016/j.jcis.2015.02.040

[14] Zhao L, Chen X, Wang X, Zhang Y, Wei W, Sun Y, *et al*. One-step solvothermal synthesis of a carbon@TiO_2 dyade structure effectively promoting visible-light photocatalysis. Adv Mater 2010; 22: 3317-21.
http://dx.doi.org/10.1002/adma.201000660

[15] Zhang J, Xiong Z and Zhao XS. Graphene–metal–oxide composites for the degradation of dyes under visible light irradiation. J Mater Chem 2011; 21: 3634-40.
http://dx.doi.org/10.1039/c0jm03827j

[16] An G, Ma W, Sun Z, Liu Z, Han B, Miao S, *et al*. Preparation of titania/carbon nanotube composites using supercritical ethanol and their photocatalytic activity for phenol degradation under visible light irradiation, Carbon 2007; 45: 1795-1801.
http://dx.doi.org/10.1016/j.carbon.2007.04.034

[17] Xue G, Liu H, Chen Q, Hills C, Tyrer M and Innocent F. Synergy between surface adsorption and photocatalysis during degradation of humic acid on TiO_2/activated carbon composites. J Hazard Mater 2011; 186: 765-72.
http://dx.doi.org/10.1016/j.jhazmat.2010.11.063

[18] Liang YY, Wang HL, Casalongue HS, Chen Z and Dai HJ. TiO_2 nanocrystals grown on graphene as advanced photocatalytic hybrid materials. Nano Res 2010; 3: 701-5.
http://dx.doi.org/10.1007/s12274-010-0033-5

[19] Zhang Y, Zhang N, Tang ZR and Xu YJ. Improving the photocatalytic performance of graphene–TiO_2 nanocomposites *via* a combined strategy of decreasing defects of graphene and increasing interfacial contact. Phys Chem Chem Phys 2012; 14: 9167-75.
http://dx.doi.org/10.1039/c2cp41318c

[20] Luia G, Liao JY, Duan A, Zhang Z, Fowler M and Yu A. Graphene-wrapped hierarchical TiO_2 nanoflower composites with enhanced photocatalytic performance. J Mater Chem A 2013; 1: 12255-62.
http://dx.doi.org/10.1039/c3ta12329d

[21] Feng Y, Feng N, Wei Y and Zhang G. An *in situ* gelatin-assisted hydrothermal synthesis of ZnO–reduced graphene oxide composites with enhanced photocatalytic performance under ultraviolet and visible light. RSC Adv 2014; 4: 7933-43.
http://dx.doi.org/10.1039/c3ra46417b

[22] Huang X, Qi XY, Boey F and Zhang H. Graphene-based composites. Chem Soc Rev 2012; 41: 666-86.
http://dx.doi.org/10.1039/C1CS15078B

[23] Fan W, Lai Q, Zhang Q and Wang Y. Nanocomposites of TiO_2 and reduced graphene oxide as efficient photocatalysts for hydrogen evolution. J Phys Chem C 2011; 115: 10694-701.
http://dx.doi.org/10.1021/jp2008804

[24] Williams G, Seger B and Kamat PV. TiO_2-graphene nanocomposites. UV-assisted photocatalytic reduction of graphene oxide. ACS Nano 2008; 2: 1487-91.
http://dx.doi.org/10.1021/nn800251f

[25] Lightcap IV, Kosel TH and PV Kamat. Anchoring semiconductor and metal nanoparticles on a two-dimensional catalyst mat. Storing and shuttling electrons with reduced graphene oxide. Nano Lett 2010; 10: 577-83.
http://dx.doi.org/10.1021/nl9035109

[26] Zhang H, Guo LH, Wang D, Zhao L and Wan B. Light-induced efficient molecular oxygen activation on a Cu(II)-grafted TiO_2/graphene photocatalyst for phenol degradation. ACS Appl Mater Interfaces 2015; 7: 1816-23.
http://dx.doi.org/10.1021/am507483q

[27] Wang J, Tsuzuki T, Tang B, Hou X, Sun L and Wang X. Reduced graphene oxide/ZnO composite: reusable adsorbent for pollutant management. ACS Appl Mater Interfaces 2012; 4: 3084-90.
http://dx.doi.org/10.1021/am300445f

[28] Thakur S, Das G, Raul PK and Karak N. Green one-step approach to prepare sulfur/reduced graphene oxide nanohybrid for effective mercury ions removal. J Phys Chem C 2013; 117: 7636-42.
http://dx.doi.org/10.1021/jp400221k

[29] Ma HL, Zhang Y, Hu QH, Yan D, Yu ZZ and Zhai M. Chemical reduction and removal of Cr(VI) from acidic aqueous solution by ethylenediamine-reduced graphene oxide. J Mater Chem 2012; 22: 5914-6.
http://dx.doi.org/10.1039/c2jm00145d

[30] Thakur S and Karak N. One-step approach to prepare magnetic iron oxide/reduced graphene oxide nanohybrid for efficient organic and inorganic pollutants removal. Mater Chem Phys 2014; 144: 425-32.
http://dx.doi.org/10.1016/j.matchemphys.2014.01.015

[31] Zhang D, Li G and Yu JC. Inorganic materials for photocatalytic water disinfection. J Mater Chem 2010; 20: 4529-36.
http://dx.doi.org/10.1039/b925342d

[32] Lee SH, Pumprueg S, Moudgil B and Sigmund W. Inactivation of bacterial endospores by photocatalytic nanocomposites. Colloids Surf B 2005; 40: 93-98.
http://dx.doi.org/10.1016/j.colsurfb.2004.05.005

[33] Ashkarran AA, Fakhari M and Mahmoudi M. Synthesis of a solar photo and bioactive CNT–TiO_2 nanocatalyst. RSC Adv 2013; 3: 18529-36.
http://dx.doi.org/10.1039/c3ra42991a

[34] Thakur S and Karak N. Green reduction of graphene oxide by aqueous phytoextracts. Carbon 2012; 50: 5331-9.
http://dx.doi.org/10.1016/j.carbon.2012.07.023

[35] Babu KS, Reddy AR, Sujatha C, Reddy KV and Mallika AN. Synthesis and optical characterization of porous ZnO. J Adv Ceram 2013; 2: 260-5.
http://dx.doi.org/10.1007/s40145-013-0069-6

[36] Akhavan O and Ghaderi E. Flash photo stimulation of human neural stem cells on graphene/TiO_2 heterojunction for differentiation into neurons. Nanoscale 2013; 5: 10316-26.
http://dx.doi.org/10.1039/c3nr02161k

[37] Ngo-Duc T, Singh K, Meyyappan M and Oye MM. Vertical ZnO nanowire growth on metal substrates. Nanotechnology 2012; 23: 194015.
http://dx.doi.org/10.1088/0957-4484/23/19/194015

[38] Barua S, Thakur S, Aidew L, Buragohain AK, Chattopadhyay P and Karak N. One step preparation of a biocompatible,

antimicrobial reduced graphene oxide–silver nanohybrid as a topical antimicrobial agent. RSC Adv 2014; 4: 9777-83. http://dx.doi.org/10.1039/c3ra46835f

[39] Chauhan I, Aggrawal S and Mohanty P. ZnO nanowire-immobilized paper matrices for visible light-induced antibacterial activity against *Escherichia coli*. Environ Sci: Nano 2015; 2: 273-9. http://dx.doi.org/10.1039/c5en00006h

Received on 05-12-2015 Accepted on 15-12-2015 Published on 31-12-2015

DOI: http://dx.doi.org/10.12974/2311-8792.2015.03.01.3